Supporting Information

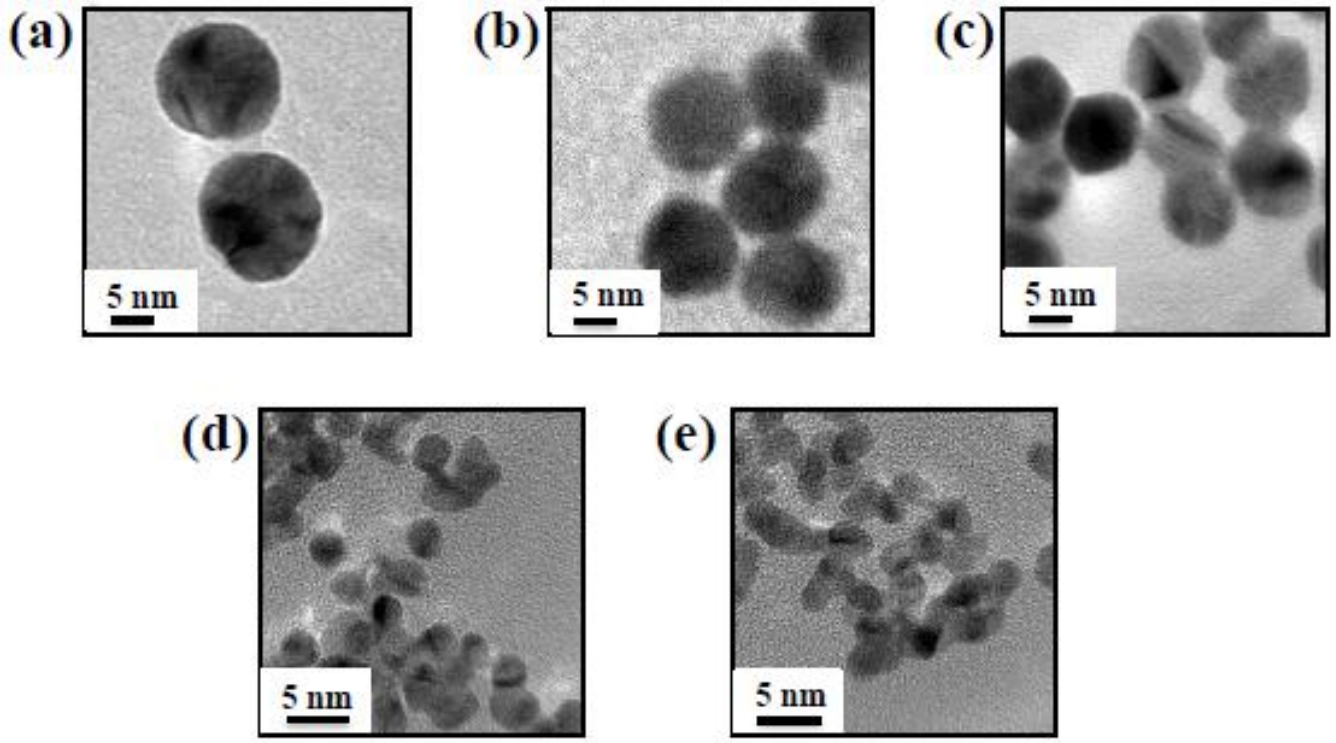

Fig. S1. TEM images depicting the enlarged view of the (a) Au NPs and (b–e) Pt/Au NPs prepared at $[Au^{3+}]/[Pt^{4+}]$ molar ratios of (b) 9.5/0.5, (c) 9.0/1.0, (d) 8.0/2.0, and (e) 7.0/3.0. Other conditions were the same as those described in Fig. 1.

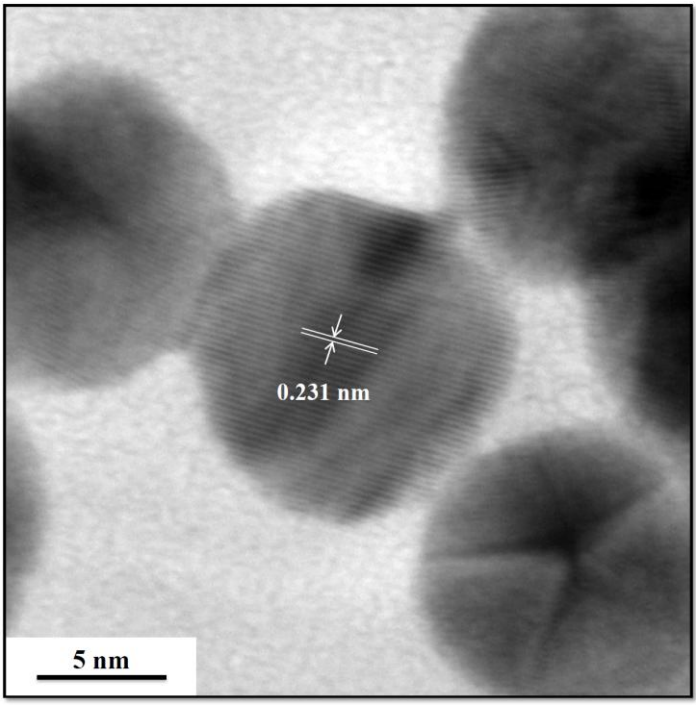

Fig. S2. High-resolution transmission electron microscopy (HR-TEM) image of $Pt_{0.1}$/Au NPs. Other conditions were the same as those described in Fig. 1.

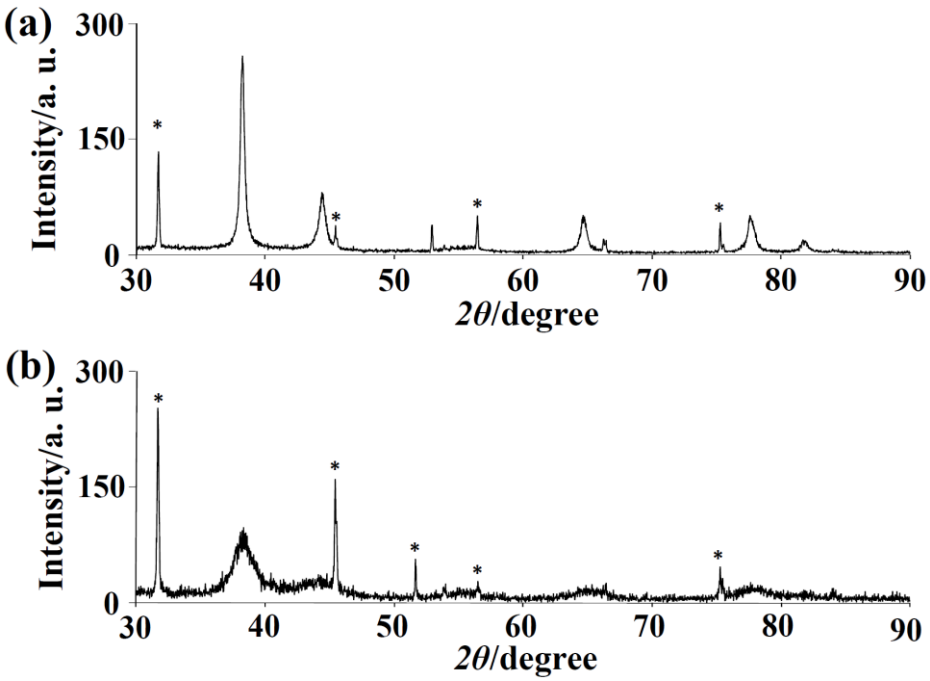

Fig. S3. XRD patterns of (a) Au NPs and (b) $Pt_{0.1}$/Au NPs. The peaks labeled with asterisks are assigned to the diffraction of the silicon wafer substrate. Other conditions were the same as those described in Fig. 1.

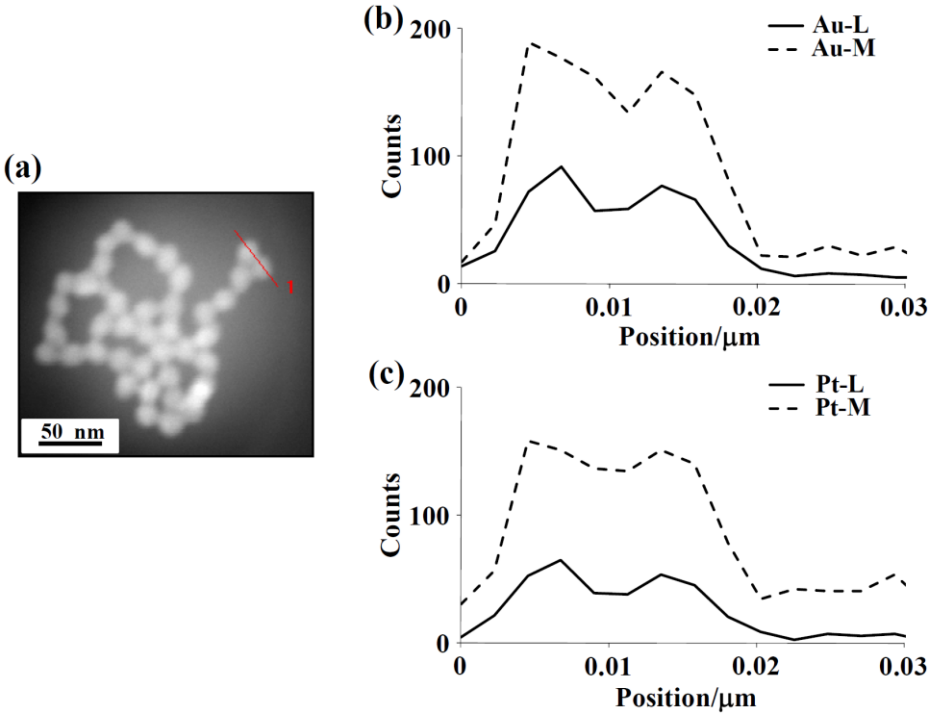

Fig. S4. (a) SEM image of $Pt_{0.1}$/Au NPs and STEM–EDS mapping of (b) Au and (c) Pt in the region marked in (a) by the red line. Other conditions were the same as those described in Fig. 1.

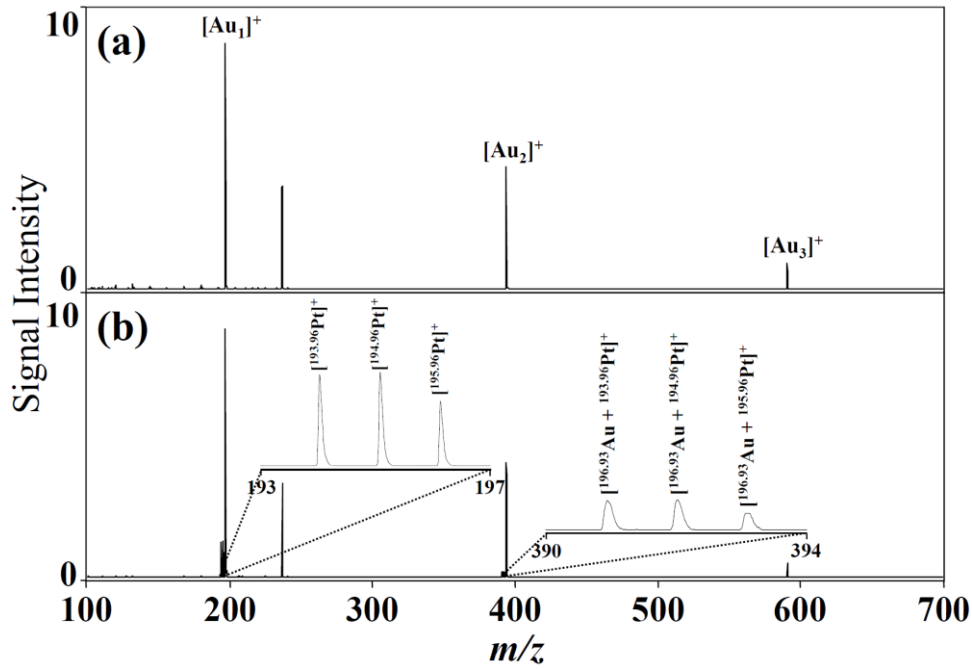

Fig. S5. SALDI-MS spectra of solutions containing (a) Au NPs (1X) and (b) $Pt_{0.1}$/Au NPs (1X) in a 5.0 mM Tris-borate solution (pH 7.0). The peaks at *m/z* 196.97, 393.93, and 590.90 in (a) are assigned to $[Au_1]^+$, $[Au_2]^+$, and $[Au_3]^+$ ions, respectively. The peaks at *m/z* 390.89, 391.89, and 392.89 in (b) correspond to $[^{196.93}Au + {}^{193.96}Pt]^+$, $[^{196.93}Au + {}^{194.96}Pt]^+$, and $[^{196.93}Au + {}^{195.96}Pt]^+$ ions, respectively. 1,000 pulsed laser shots were applied, and we accumulated the signals from 10 MALDI target positions under a laser fluence of 45 μJ. Other conditions were the same as those described in Fig. 1.

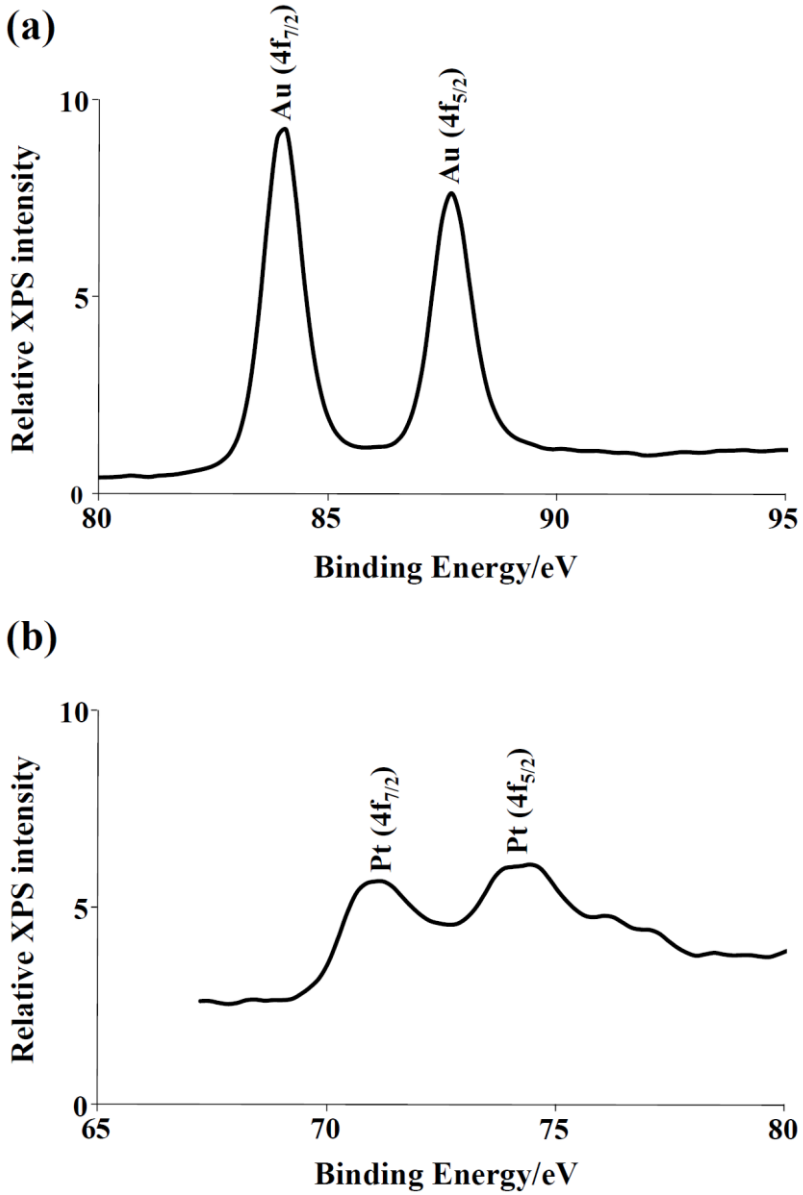

Fig. S6. (a) Au 4f and (b) Pt 4f core-level photoelectron spectra of $Pt_{0.1}$/Au NPs applied onto silicon substrates and measured at room temperature. Other conditions were the same as those described in Fig. 1.

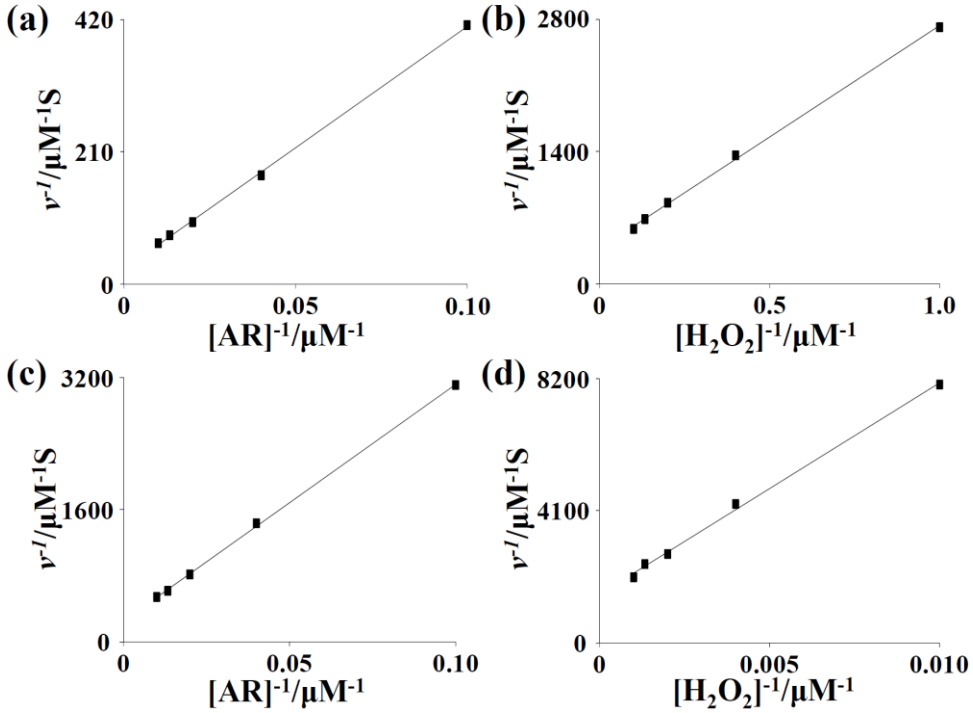

Fig. S7. Double reciprocal plots of activity of (a), (b) HRP and (c), (d) $Pt_{0.1}$/Au NPs with the concentration of one substrate fixed and the other [(a), (c) AR or (b), (d) H_2O_2] varied. The velocity (v) of the reaction was measured using (a), (b) 0.15 nM HRP or (c), (d) 0.01X $Pt_{0.1}$/Au NPs in a 5.0-mM Tris-borate solution (pH 7.0). (a), (c) The concentration of H_2O_2 was 0.5 mM for HRP or 2.5 mM for $Pt_{0.1}$/Au NPs, and the AR concentration was varied. (b), (d) The concentration of AR was 10 μM and the H_2O_2 concentration was varied. Other conditions were the same as those described in Fig. 3.

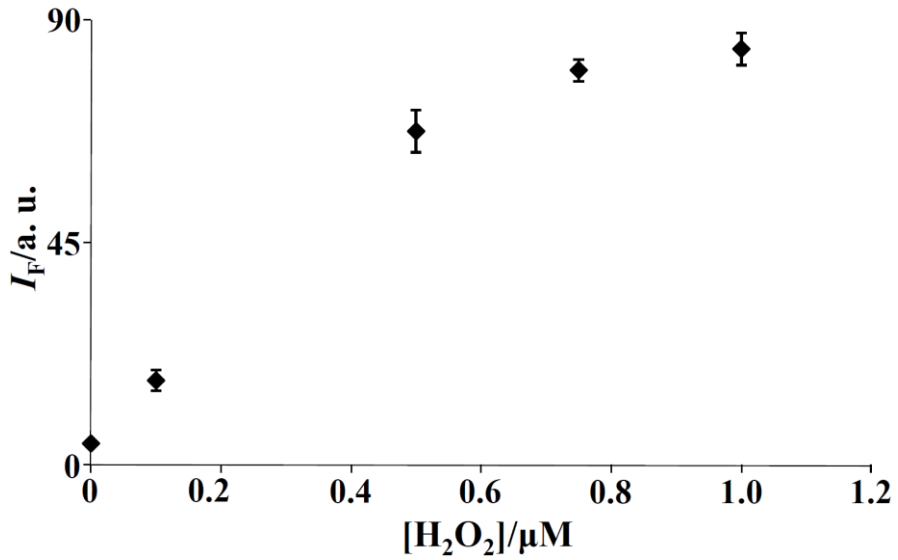

Fig. S8. Plot of fluorescence intensity of Tris-borate solutions (5 mM, pH 7.0) containing AR (10 μM) and $Pt_{0.1}$/Au NPs (0.01X) at 585 nm in the presence of H_2O_2 (0–1.0 μM); error bars represent the standard deviations from three repeated experiments.

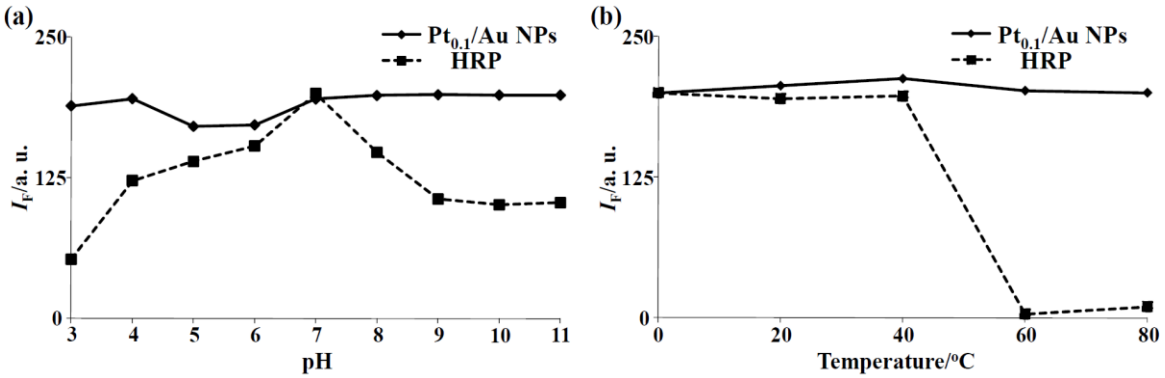

Fig. S9. Comparison of the stability of $Pt_{0.1}$/Au NPs and HRP. (a) $Pt_{0.1}$/Au NPs or HRP were first incubated in sodium phosphate solution at pH 3–11 for 2 h, and then, their peroxidase activities were measured under the conditions described in Fig. 3. (b) $Pt_{0.1}$/Au NPs or HRP were first incubated at 0–80 °C for 2 h, and then, the peroxidase activity was measured under the conditions described in Fig. 3.

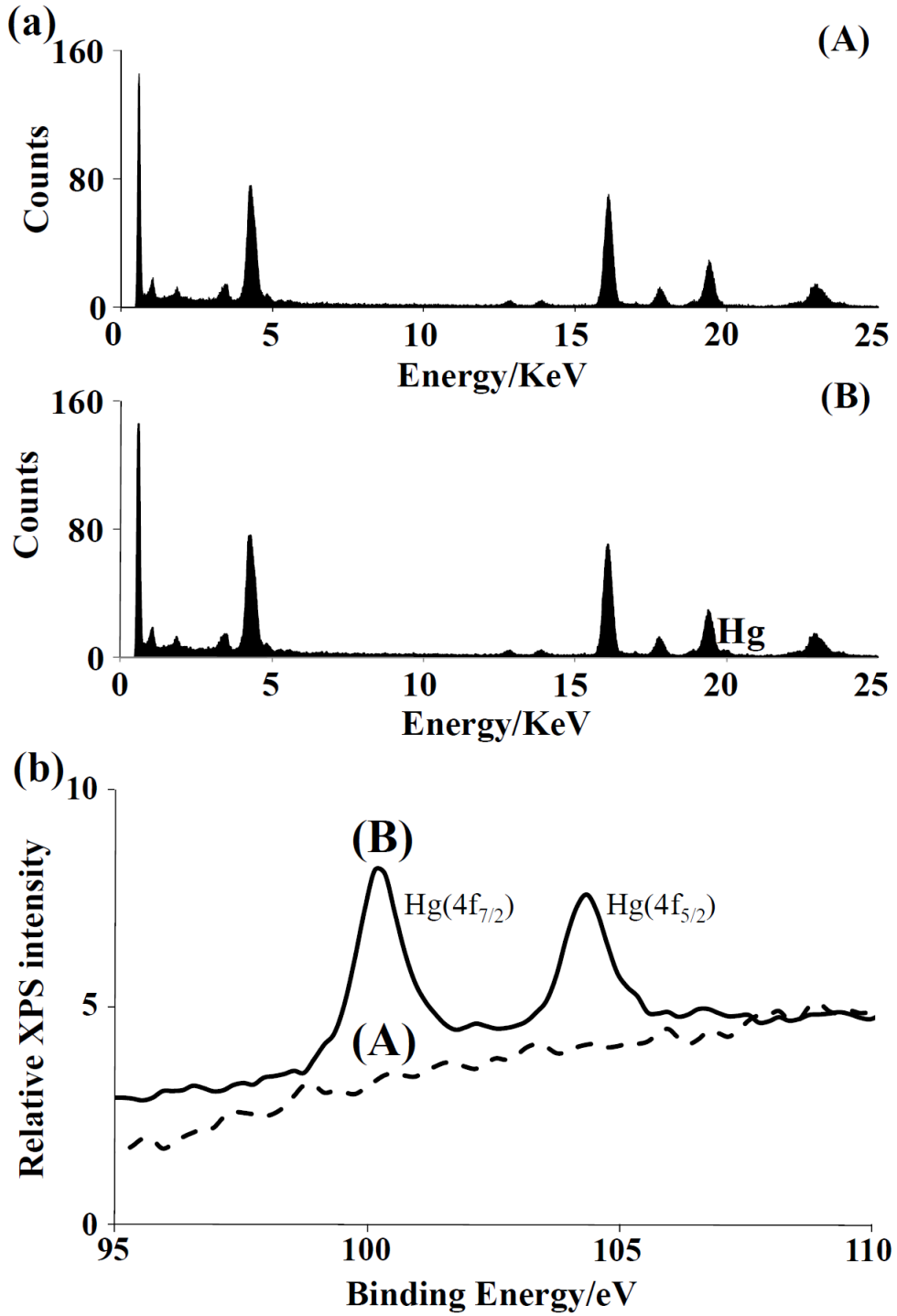

Fig. S10. (a) EDS and (b) XPS spectra of $Pt_{0.1}$/Au NPs (0.01X) in the (A) absence and (B) presence of Hg^{2+} (10 μM). Other conditions were the same as those described in Fig. 4.

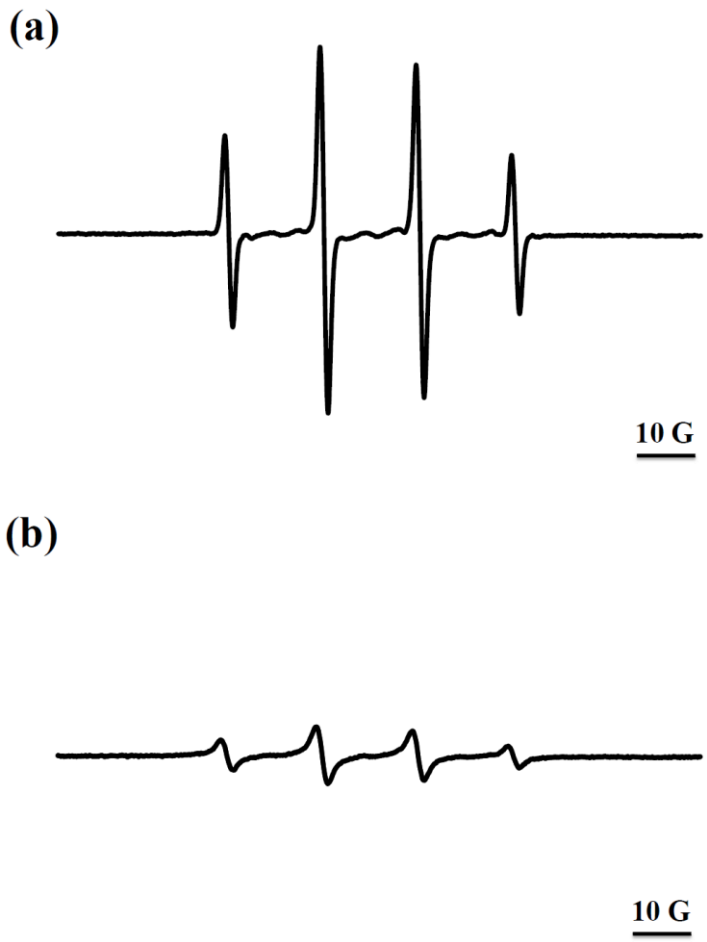

Fig. S11. EPR spectra of hydroxyl radicals in the systems of (a) DMPO (50 mM) and H_2O_2 (50 mM), and $Pt_{0.1}$/Au NPs (0.1X) and (b) DMPO (50 mM), H_2O_2 (50 mM), $Pt_{0.1}$/Au NPs (0.1X), and Hg^{2+} (10 μM). Samples were exposed to 15 min of UV light at 270 nm. EPR experiments were run on a Bruker EMX spectrometer. EPR conditions: microwave power, 1 mW; field modulation, 1 G; scan width, 100 G. Other conditions were the same as those described in Fig. 4.

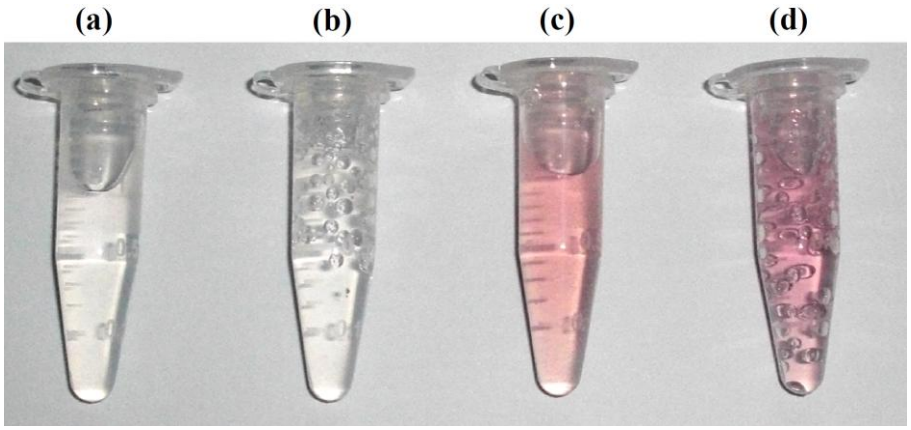

Fig. S12. Photograph of 5.0-mM Tris-borate solution (pH 7.0) containing (a) 50 mM H_2O_2; (b) 50 mM H_2O_2 and catalase (1.5 nM ≈ 0.13 unit/mL); (c) 50 mM H_2O_2 and $Pt_{0.1}$/Au NPs (0.1X ≈ 2 nM); and (d) 50 mM H_2O_2, $Pt_{0.1}$/Au NPs (0.1X ≈ 2 nM), and Hg^{2+} (10 μM). Incubation, 20 min. Addition of Hg^{2+} into the mixture of H_2O_2 and $Pt_{0.1}$/Au NPs results in the acceleration of bubble formation (vial d). Other conditions were the same as those described in Fig. 4.

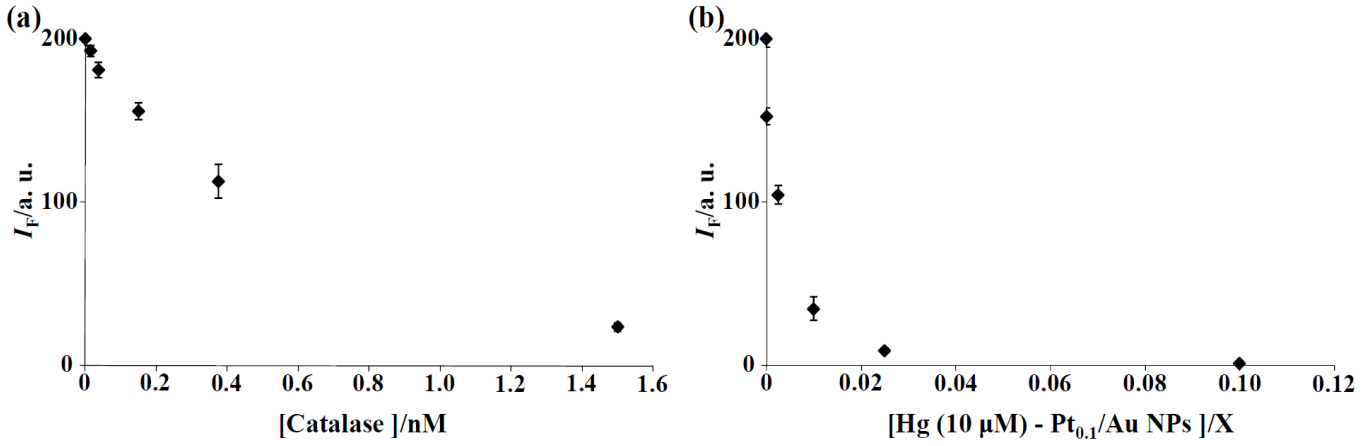

Fig. S13. Detection of the activity of (a) catalase and (b) Hg–$Pt_{0.1}$/Au NPs using the Amplex® UltraRed reagent-based assay. The activity of 1.0 nM catalase is about 0.087 unit/mL. The concentration of 0.1X $Pt_{0.1}$/Au NPs is about 2.0 nM. Initially, each reaction contained the indicated amounts of catalase or Hg (10 μM)–$Pt_{0.1}$/Au NPs and 10 μM H_2O_2 in a 5.0 mM Tris-borate solution (pH 7.0) and was incubated for 30 min. The final reaction solutiom containing Amplex® UltraRed (10 μM) and 1.32 U/mL HRP was incubated at 37°C. After 30 min, fluorescence was measured in a fluorescence microplate reader using excitation at 530 nm and fluorescence detection at 590 nm. Error bars represent the standard deviations from four repeated experiments.

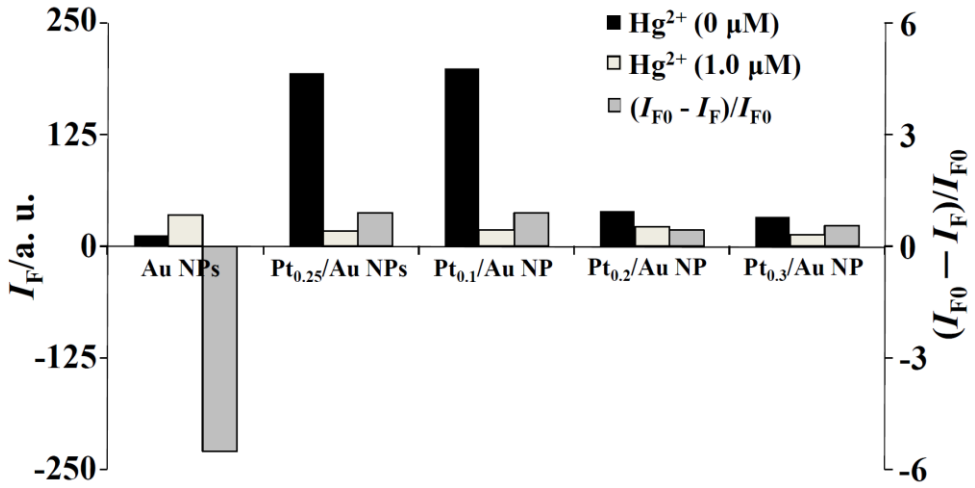

Fig. S14. Fluorescence intensities (at 585 nm) of a 5-mM Tris-borate solution (pH 7.0) containing 50 mM H_2O_2, AR (10 μM) and various Au NPs or $Pt_{0.1}$/Au NPs in the absence (black bar, I_{F0}) and presence of 1.0 μM Hg^{2+} (white bar, I_F). Relative fluorescence increases [gray bar, $(I_{F0} - I_F)/I_{F0}$] at 585 nm of the probe for detection of Hg^{2+} (1.0 μM). Other conditions were the same as those described in Fig. 4.

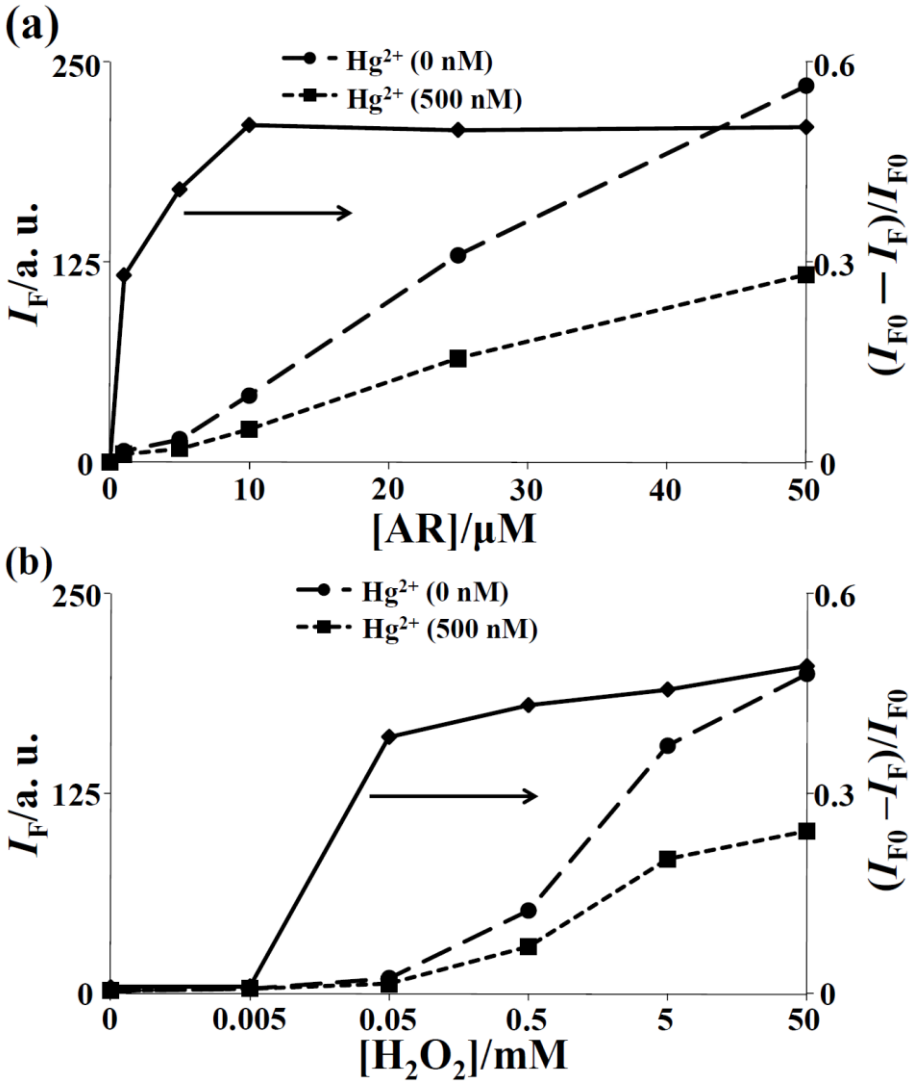

Fig. S15. Effect of the concentration of (a) AR and (b) H_2O_2 on the detection of Hg^{2+} (500 nM) by AR–$Pt_{0.1}$/Au NPs probe. I_{F0} and I_F are the fluorescence intensities of the AR–$Pt_{0.1}$/Au NPs (0.01X) solution in the absence and presence of Hg^{2+}, respectively. Other conditions were the same as those described in Fig. 4.

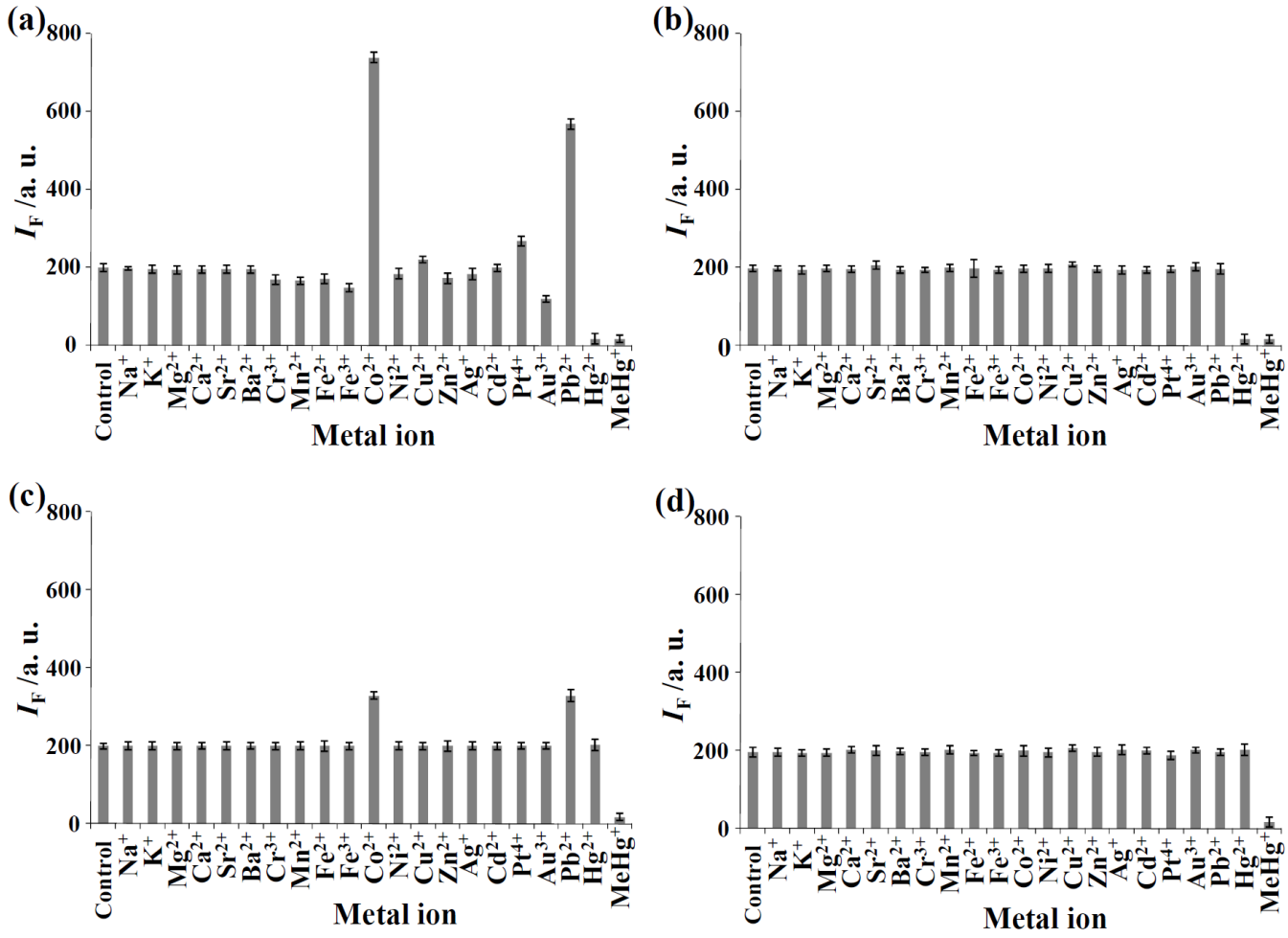

Fig. S16. Selectivities of the AR–$Pt_{0.1}$/Au NPs sensor for different metal ions (1.0 μM) and mercury species (1.0 μM) in the (a) absence and presence (b–d) of masking agents (b) 0.1% PAA, (c) 0.3 nM Te NW, and (d) 0.1% PAA and 0.3 nM Te NW. Error bars represent the standard deviations from five repeated experiments. Other conditions were the same as those described in Fig. 4.

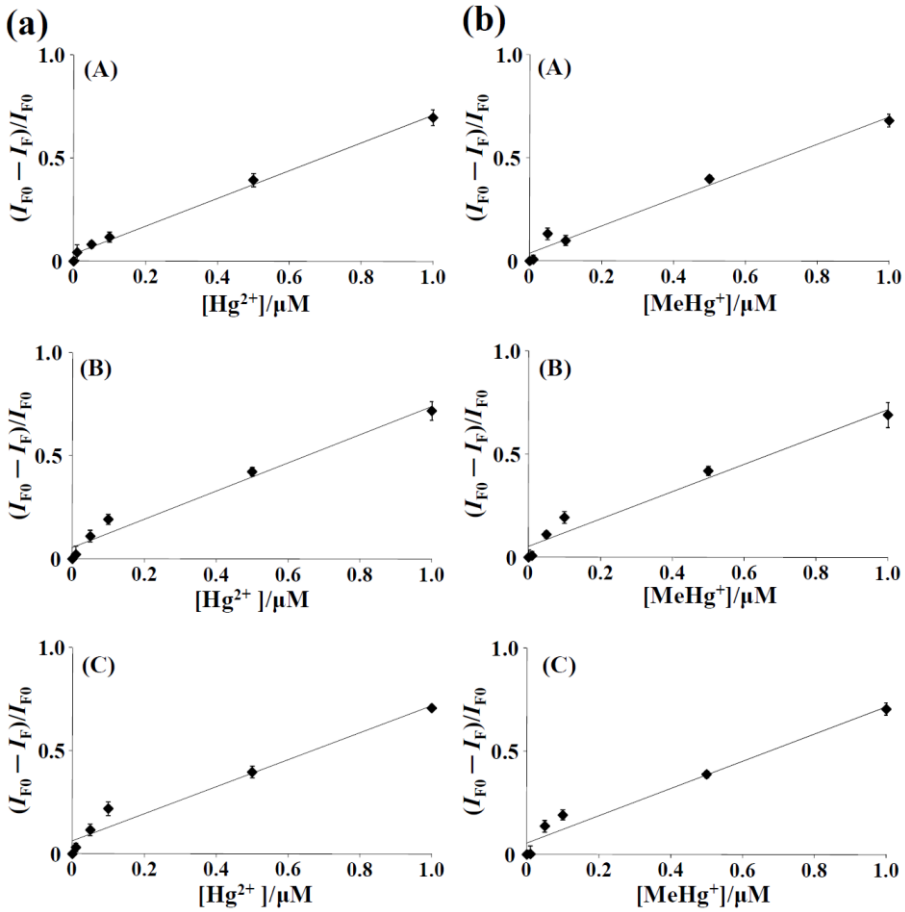

Fig. S17. Analyses of representative (A) tap water, (B) pond water, and (C) stream water samples using (a) AR–$Pt_{0.1}$/Au NPs–PAA and (b) AR–$Pt_{0.1}$/Au NPs–PAA/Te NWs probes for Hg^{2+} and $MeHg^+$, respectively. Diluted water samples (twofold) were spiked with Hg^{2+} (0–1.0 μM) and $MeHg^+$ (0–1.0 μM), respectively. Other conditions were the same as those described in Fig. 5.